Original Article

Ultrasound propagation characteristics within the bone tissue of miniature ultrasound probes: implications for the spinal navigation of pedicle screw placement

Peiyang Li[1]^, Suoyuan Li[2], Zhiqiang Li[2], Wenjia Lu[3], Weiwei Shao[4], Zhangjian Li[4], Yiwen Xu[4], Hong Zhang[2], Bin Ju[5], Jun Shen[2,6], Yaoyao Cui[1]

[1]Academy for Engineering & Technology, Fudan University, Shanghai, China; [2]Department of Orthopeadics, The Affiliated Suzhou Hospital of Nanjing Medical University, Suzhou Municipal Hospital, Gusu School, Nanjing Medical University, Suzhou, China; [3]Suzhou GuoKe Ultra Medical Technology Co., Ltd., Suzhou, China; [4]Suzhou Institute of Biomedical Engineering and Technology, Chinese Academy of Sciences, Suzhou, China; [5]College of Electrical Engineering and Automation, Anhui University, Hefei, China; [6]Suzhou Key Laboratory of Orthopedic Medical Engineering, Suzhou, China

Contributions: (I) Conception and design: P Li; (II) Administrative support: J Shen, Y Cui; (III) Provision of study materials or patients: P Li, S Li, H Zhang; (IV) Collection and assembly of data: P Li, W Lu, Y Xu, B Ju; (V) Data analysis and interpretation: P Li, W Shao, Z Li, S Li; (VI) Manuscript writing: All authors; (VII) Final approval of manuscript: All authors.

Correspondence to: Yaoyao Cui, PhD. Academy for Engineering & Technology, Fudan University, No. 220, Handan Road, Yangpu District, Shanghai 200240, China. Email: cuiyy@sibet.ac.cn; Jun Shen, MD. Department of Orthopeadics, The Affiliated Suzhou Hospital of Nanjing Medical University, Suzhou Municipal Hospital, Gusu School, Nanjing Medical University, No. 26, Daoqian Street, Gusu District, Suzhou 215008, China; Suzhou Key Laboratory of Orthopedic Medical Engineering, Suzhou, China. Email: 18112603158@163.com.

Background: The accuracy of pedicle screw fixation is crucial for patient safety. Traditional navigation methods based on computed tomography (CT) imaging have several limitations. Therefore, this study aimed to investigate the ultrasonic propagation characteristics of bone tissue and their relationship with CT imaging results, as well as the potential application of ultrasound navigation in pedicle screw fixation.

Methods: The study used three bovine spine specimens (BSSs) and five human vertebral allograft bones (HABs) to progressively decrease the thickness of the cancellous bone layer, simulating the process of pedicle screw perforation. Five unfocused miniature ultrasound probes with frequencies of 2.2, 2.5, 3, 12, and 30 MHz were employed for investigating the ultrasonic propagation characteristics of cancellous and cortical bone through ultrasound transmission and backscatter experiments. The CT features of the bone tissue was obtained with the Skyscan 1174 micro-CT scanner (Bruker, Billerica, MA, USA).

Results: The experimental results demonstrated that low-frequency (2–3 MHz) ultrasound effectively penetrated the cancellous bone layer up to a depth of approximately 5 mm, with an attenuation coefficient below 10 dB/cm. Conversely, high-frequency (12 MHz) ultrasound exhibited significant signal attenuation in cancellous bone, reaching up to 55.8 dB/cm. The amplitude of the backscattered signal at the cancellous bone interface exhibited a negative correlation with the bone sample thickness (average r=–0.84), meaning that as the thickness of the cancellous bone layer on the cortical bone decreases, the backscattered signal amplitude gradually increases ($P<0.05$). Upon reaching the cortical bone interface, there was a rapid surge in echo signal amplitude, up to 8 times higher. Meanwhile, the statistical results indicated a significant correlation between the amplitude of the echo signal and the micro-CT scanning results of bone trabecular structure.

Conclusions: Theoretically, using multiple ultrasonic probes (≥3) and regions of interest (ROIs) (≥5) has the potential to provide surgeons with early warning signals for pedicle perforation based on three or more

^ ORCID: 0000-0003-0280-9922.

successive increases in echo signal amplitude or a sudden substantial increase. The statistical results indicate a significant correlation between the amplitude of the echo signal and the micro-CT scanning results of bone trabeculae, suggesting the potential use of ultrasound as opposed to CT for real-time intraoperative bone navigation.

Keywords: Ultrasonic propagation characteristics; micro-computed tomography (micro-CT); cancellous bone; pedicle screw; echo signal amplitude

Submitted Feb 26, 2024. Accepted for publication May 15, 2024. Published online Jun 27, 2024.
doi: 10.21037/qims-24-377
View this article at: https://dx.doi.org/10.21037/qims-24-377

Introduction

Pedicle screw fixation is widely employed in spinal posterior stabilization procedures across various clinical scenarios, including spinal deformity, trauma, tumor, and degenerative diseases (1,2). However, once the screw penetrates out from the pedicle during the surgical procedure, it inevitably causes inadvertent injury to adjacent vital structures including the spinal cord, nerve roots, and blood vessels, and other critical adjacent structures (3-5). This can in turn potentially lead to complications such as paralysis, ischemia of the brain stem or cerebellum, and even aortic perforation in severe cases. The accurate guidance of screw implantation orientation and depth is thus of utmost importance (6). The conventional freehand technique relies on anatomical landmarks and X-ray images as references for positioning. The success rate and quality of screw placement primarily depend on the surgeon's tactile perception and experience. Research has indicated that in cases of idiopathic scoliosis, the incidence of pedicle screw breach larger than 2 mm from the freehand technique ranges from 6.5% to 33.9% (7-9). The use of intraoperative C-arm fluoroscopy-assisted screw placement is currently prevalent in clinical practice. However, due to the acquisition of two-dimensional images, the provided information is limited, leading to relatively elevated rates of screw penetration (10). Moreover, there exists a potential hazard of ionizing radiation exposure for both patients and medical personnel. The implementation of computer-assisted navigation (CAN) systems has significantly enhanced the precision and safety of surgical procedures (11). However, certain challenges still persist, including the high cost of equipment, relatively intricate operation processes, requirement of substantial physical space and susceptibility to environmental interference. Additionally, registration is necessary to establish the correspondence between the images and the anatomical location of the patient during surgery. Position changes can easily lead to registration errors. Although advanced navigation technologies such as O-arm navigation can provide immediate intraoperative three-dimensional (3D) computed tomography (CT) images and perform fully automatic registration, there are certain drawbacks, including an increased scanning time and repeated radiation exposure during surgery (12). Robot-assisted techniques incurs higher costs while offering comparable accuracy (13) in screw placement to the aforementioned navigation devices.

Therefore, it is imperative to develop a clinically safer method capable of continuous and real-time monitoring of screw placement position and depth. The use of ultrasound in orthopedics is regarded as a promising novel approach due to its inherent advantages (14-16), including the absence of ionizing radiation, nondestructive nature, cost-effectiveness, portability, and real-time imaging capabilities. When the ultrasound signal is incident on the cancellous bone interface, a portion of the energy penetrates into the interior of the cancellous bone while another portion is reflected at this interface (17). High-frequency ultrasound offers superior resolution but also involves significant attenuation, with most of the incident wave being attenuated within cancellous bone. On the other hand, low-frequency ultrasound provides strong penetration capability despite lower image resolution (18). In our previous paper (19), we proposed that combining high-frequency and low-frequency ultrasound can enable high-resolution imaging with deep tissue detection. However, we could not draw a definitive conclusion regarding the optimal frequency range, transducer size, or power required for achieving deep detection in cancellous bone. Therefore, a comprehensive understanding of the ultrasonic propagation characteristics

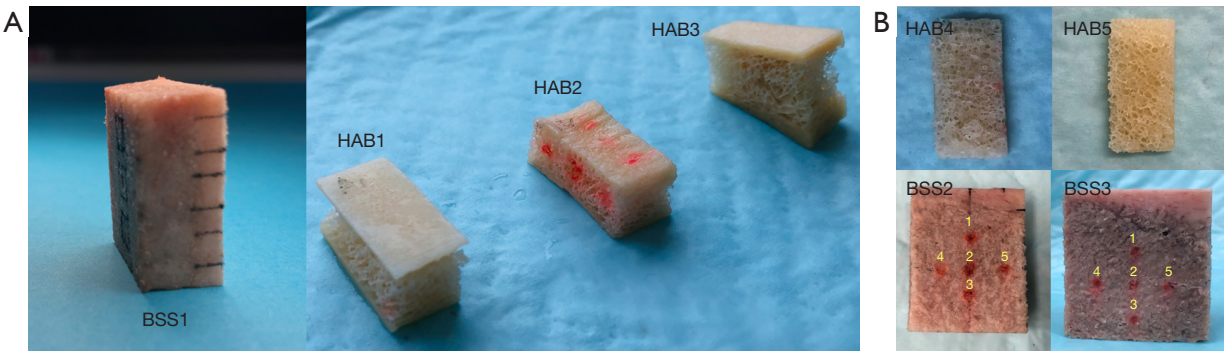

Figure 1 Experimental bone samples. (A) Bone samples for the ultrasound backscatter experiment and (B) bone samples for the ultrasound transmission experiment. BSS, bovine spine specimen; HAB, human vertebral allograft bone.

of cancellous bone across various ultrasound frequencies remains elusive.

In this study, we investigated the ultrasonic transmission and backscattering characteristics of bovine and human cancellous bone samples using ultrasonic transducers of varying frequencies. We examined the attenuation coefficient and sound velocity of ultrasonic propagation in bones; evaluated the impact of probe frequency, size, and performance on the depth of ultrasonic penetration in cancellous bones; and observed the amplitude of echo wave. Finally, the feasibility of ultrasound-guided navigation in clinical spinal pedicle surgery was ascertained.

Methods

Materials

The literature (20) suggests that the average diameter of the L1–L5 lumbar vertebral pedicles in human body ranges from 6 to 15 mm, with the average width of the L5 vertebra being around 15 mm. Therefore, to simulate the scenario of pedicle perforation in the lumbar vertebrae, the trabecular bone thickness should be at least 6 mm. Furthermore, to avoid interference from sample boundaries, it is essential to select bone samples with large, flat interfaces that are easily accessible. Additionally, it is advisable to maintain uniform cortical bone thickness. The bone samples used in this study were all custom-made. The bone specimens included in this study included fresh bovine spine specimens (BSSs) (Animal Experiment Center of Nanjing Medical University, Nanjing, China) and human vertebral allograft bones (HABs) (Shanxi Osteorad Biological Materials Co., Ltd., Taiyuan, China); registration certificate number: 20163460428), the latter of which were prepared from human bone tissue that had been deep-frozen, decorticated, defatted, freeze-dried, and sterilized with Co-60 gamma irradiation to reduce immunogenicity. As shown in *Figure 1*, the bone samples used in this study were commercial bone blocks and did not involve any animal or human experimentation. Therefore, it was not necessary to obtain approval from the Animal Ethics Review Board and the Human Research Ethics Committee.

(I) Backscatter experiment: A table saw (MBS 240/E; Proxxon, Föhren, Germany) was used to surgically remove the cortical bone and a portion of the cancellous bone from one side of BSS1 and HAB1–3, with the remaining half of cancellous and cortical bone being preserved. The thickness of BSS1 and HAB1–2 was approximately 8.00 mm. Due to the intricate structure of HAB3, the remaining thickness was only about 6.5 mm. In the ultrasonic backscatter experiment, to simulate the different distances from the boreholes in the pedicles to outside walls during clinical pedicle screw implantation, we gradually reduced the cancellous bone thickness of the bone sample in a layered manner, with each layer being decreased by approximately 2 mm, as shown in *Figure 2*. Ultimately, only cortical bone remained, and the simulated screw trajectory closely approximated cortical bone.

(II) Transmission experiment: The cortical bones were removed from both sides of BSS2–3 and HAB4–5, leaving behind cancellous bone with a thickness of 8.00 mm. BSS2–3 were successively thinned from 8.00 to 7.00 mm, 6.5, 5.00, and 2.00 mm, respectively. HAB4–5 were successively thinned from 8.00 to 6.50 mm, 5.00, 3.00, and 2.00 mm, respectively. The

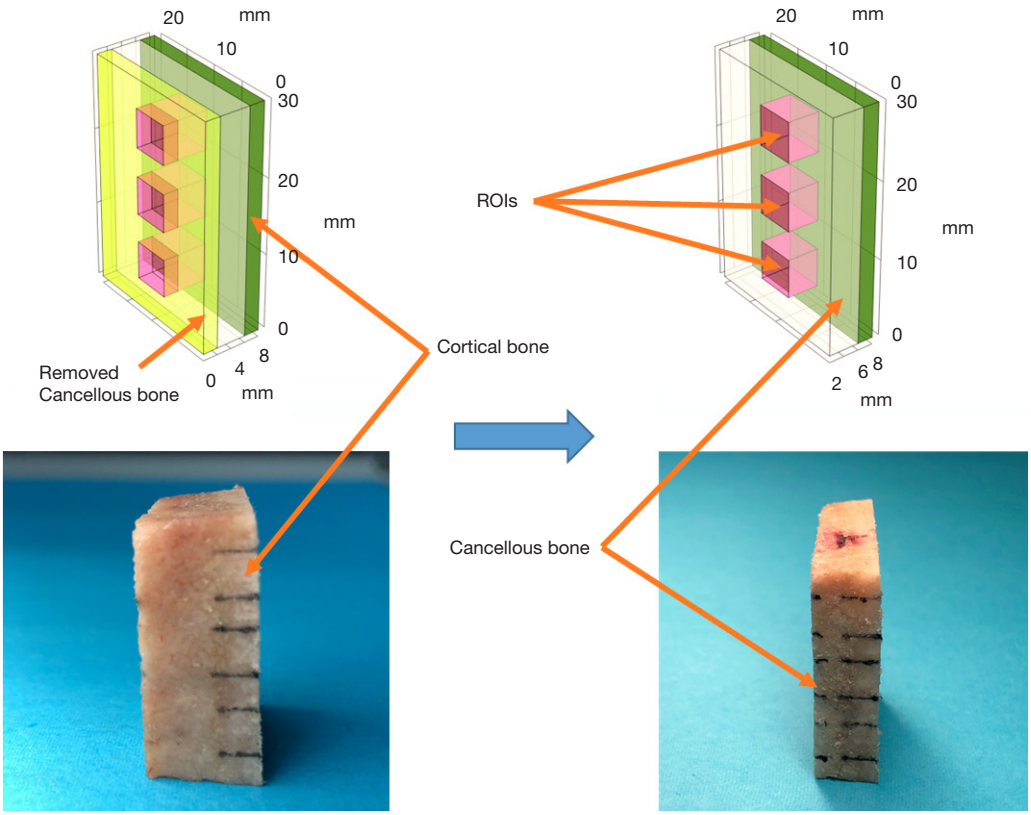

Figure 2 Schematic representation of the reduction in cancellous bone thickness and physical illustrations of bone specimens. ROI, region of interest.

Table 1 Thickness parameter of the bone blocks

Experiment	Bone	Cancellous bone thickness (mm)					Cortical bone thickness (mm)
		No. 1	No. 2	No. 3	No. 4	No. 5	
Backscatter experiment	BSS1	8	6.5	5	3	–	2
	HAB1	8	6	4	–	–	1
	HAB2	8	6	4	–	–	1.5
	HAB3	6.5	4	–	–	–	2
Transmission experiment	BSS2	8	7	6.5	5	2	–
	BSS3	8	7	6.5	5	2	–
	HAB4	8	6.5	5	3	2	–
	HAB5	8	6.5	5	3	2	–

BSS, bovine spine specimen; HAB, human vertebral allograft bone.

thickness parameters of the bone blocks are shown in *Table 1*. The bone blocks were repeatedly immersed and rinsed in normal saline solution and then immersed in a degassed water environment for over 30 minutes to eliminate potential air bubbles within the cancellous bone samples.

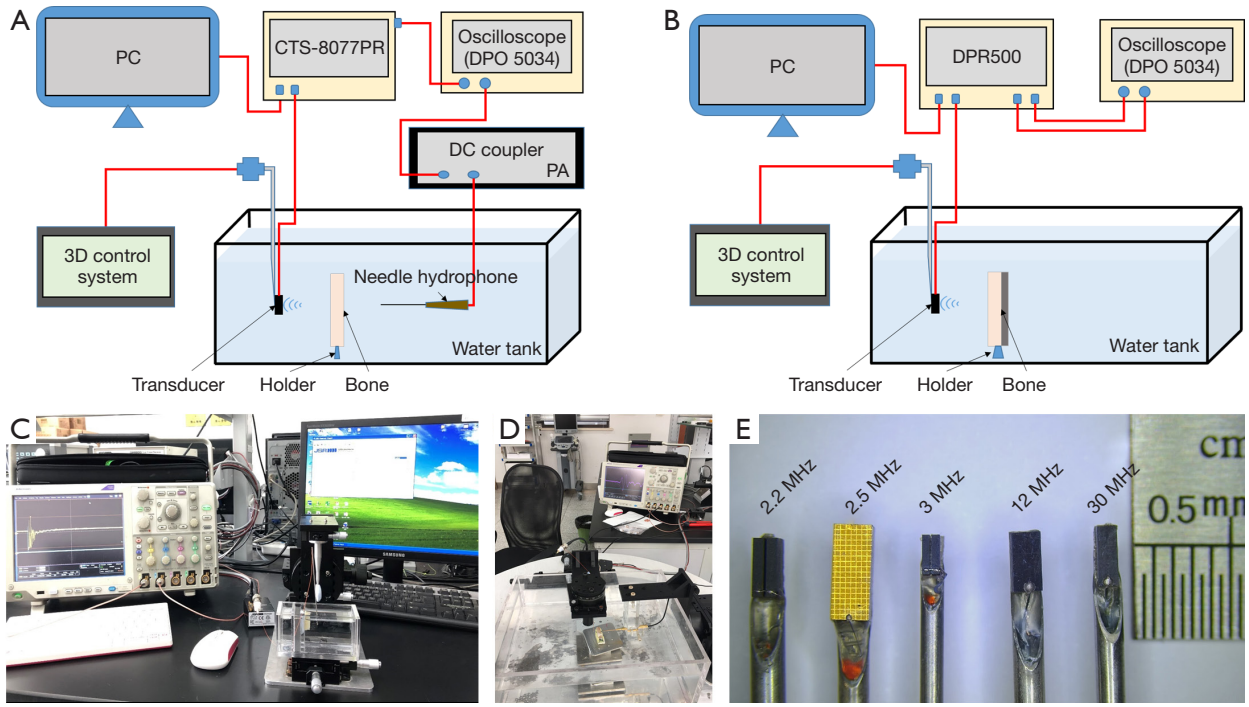

Figure 3 The experimental systems. (A) Schematic diagram of the transmission experiment setup. (B) Schematic diagram of the backscatter experiment setup. (C) Experimental setup for the backscattering measurements. (D) Experimental setup for the transmission measurements. (E) The ultrasound transducers employed in the experiment: 2.2, 2.5, 3, 12, and 30 MHz from left to right, respectively. PC, personal computer; DC, direct current; PA, precision acoustic; 3D, three-dimensional.

Experimental platform

The experimental setup comprised a customized ultrasonic immersion transmission system and backscattering measurement system, as shown in *Figure 3A-3D*. The experimental platform contained: a four-dimensional mobile control system (homemade), a transparent acrylic water tank (customized), a bone sample fixing bracket (customized), an ultrasonic pulse transmitter/receiver (CTS-8077PR; Guangdong Shantou Ultrasonic Electronics Co., Ltd., Shantou, China), an ultrasonic pulse transmitter/receiver device (DPR 500; Imaginant, Ltd., Pittsford, NY, USA), a broadband ultrasonic signal receiver needle hydrophone (NH0500;Precision Acoustics Ltd., Dorchester, UK), an oscilloscope (DPO 5034; Tektronix, Beaverton, OR, USA), and a host computer. The performance parameters of the ultrasonic probes (*Figure 3E*; Suzhou Guoke Angzhuo Medical Technology Co., Ltd., Suzhou, China) employed in the experiment are presented in *Table 2*. Medical syringe needles with a diameter of 1.8–2.5 mm were used to fix the microultrasound transducers as the intraoperative pedicle probe. DPR 500 (Imaginant Inc., Pittsford, NY, USA) was employed as the ultrasonic system.

The experiments were conducted in a controlled environment of deionized and degassed water at a temperature of approximately 25 ℃, with the speed of sound measured at 1,500 m/s. The bone samples were secured in place using a holder during the experiment. The ultrasound probe and needle hydrophone were coaxially positioned on either side of the bone specimen in the experiment involving ultrasound transmission, as shown in *Figure 3A*. The needle hydrophone was installed on a customized fixture, ensuring optimal stability during movement. The ultrasonic probe was securely affixed to the control platform, enabling precise X-axis translation, pitch adjustment in the X-Y plane, and rotation around the Z-axis. The relative positioning between the probe and the bone sample was precisely adjusted using a 3D control system for fixing the probe and a two-dimensional (2D) console for securing the tank. Through this experimental setup, transmission or backscatter measurements could be conducted at the multiple regions of interest (ROIs) on the same

Table 2 The performance characteristics of the ultrasonic probes

No.	Center frequency (MHz)	Bandwidth (–6 dB)	Dimensions
1	2.2	44.36%	3.0 mm × 1.3 mm × 2.0 mm
2	2.5	50.08%	5.0 mm × 2.0 mm × 2.5 mm
3	3	48.26%	2.0 mm × 0.9 mm × 1.6 mm
4	12	52.67%	3.0 mm × 1.0 mm × 0.8 mm
5	30	26.91%	3.0 mm × 1.0 mm × 0.9 mm

cancellous bone sample, thereby minimizing experimental measurement errors. The ROIs were confined within the sample boundary, with a distance of approximately 5 mm from the edge being maintained to ensure that the ultrasound beam's main lobe lay entirely in the plane of the bone sample being measured, thereby avoiding any potential influence from scattering or diffracted ultrasound signals emanating from the sample boundary. To eliminate the influence of the ultrasonic incidence angle, we adjusted the relative spatial positions of the bone sample and the ultrasound transducer by fine-tuning the four-dimensional control system during the signal acquisition. When the amplitude of the acquired ultrasound signal reached its maximum, we determined that the ultrasound signal was vertically incident. The transmission experiments involved four ROIs for the BSSs and three ROIs for the HAB samples at each thickness level. The transmission experiments were conducted at frequencies of 2.2, 2.5, 3, and 12 MHz, encompassing a total of 160 ROIs in BSS samples and 120 ROIs in HAB samples.

In the backscatter experiment, following each reduction of cancellous bone thickness in BSS1, 3 ROIs were determined, with a total of 60 ROIs. Due to the variable orientation of trabecular bone within the same bone sample, significant differences were observed in echo amplitudes across different regions. Consequently, 5 ROIs were selected for ultrasound echo testing, and a total of 165 ROIs were recorded. The transmitted ultrasound signal was received by the needle hydrophone, while the backscattered ultrasound signal was acquired by the pulse transmitter/receiver. The acquired signals were then displayed on an oscilloscope and saved as a csv file for subsequent data processing. Data analysis was performed using GraphPad Prism 10.0 software (GraphPad Software, La Jolla, CA, USA). One-way analysis of variance (ANOVA) was use to compare group differences, the least significant difference (LSD) test for homogeneity of variance or Dunnett's T3 for heterogeneity of variance was applied for multiple comparisons. Statistical significance was set at a P value <0.05.

Experimental data processing and analysis

(I) The ultrasonic transmission characteristics of cancellous bone were measured using the standard substitution method. The speed of sound in cancellous bone sample and water is $v(f)$ and c_w (1497 m/s), respectively. The time shift of the received pulse caused by sample insertion is $\varphi(f)$, and thus the speed of sound ($v(f)$) of tissue sample can be calculated as follows:

$$v(f)=\frac{1}{\frac{1}{c_w}-\frac{\varphi(f)}{D}} \quad [1]$$

The attenuation (21) was calculated as follows:

$$\alpha(f)=\frac{20\log\left(A_{sig}(f)/A_{ref}(f)\right)}{D} \quad [2]$$

where $\alpha(f)$ is the measured attenuation coefficient; $A_{sig}(f)$ and $A_{ref}(f)$are the amplitude spectrum of the reference signal and the transmission signal, respectively; and D is the sample thickness. The formulation of the attenuation coefficient [2], assumes negligible diffraction loss due to well-matched phase speeds between deionized water and cancellous bone (22). Furthermore, transmission losses at the interface (resulting from reflection and wave mode conversion) are also considered insignificant (23,24).

(II) When a transducer is used for detection and imaging in a confined space, it becomes susceptible to interference from the reflected waves of the surrounding walls and lateral and back radiation signals from the transducer, resulting in a diminished signal-to-noise ratio of the echo signal, compromised imaging quality, and challenges in distinguishing tissue structures. Simultaneously, the near-field blind area of the transducer also hampers detection and imaging within this limited space. The reflected signals originating from tissues closest to the transducer are submerged within its near-field blind area, rendering them indistinguishable. Consequently, in this study, cancellous bone echo signal was extracted by filtering out a reference signal from the first echo signal. Specifically, prior to insertion of the bone sample, reference signals devoid of any echo information were acquired. Subsequently, after insertion of the bone sample was completed, echo signals specific to that particular bone sample were acquired.

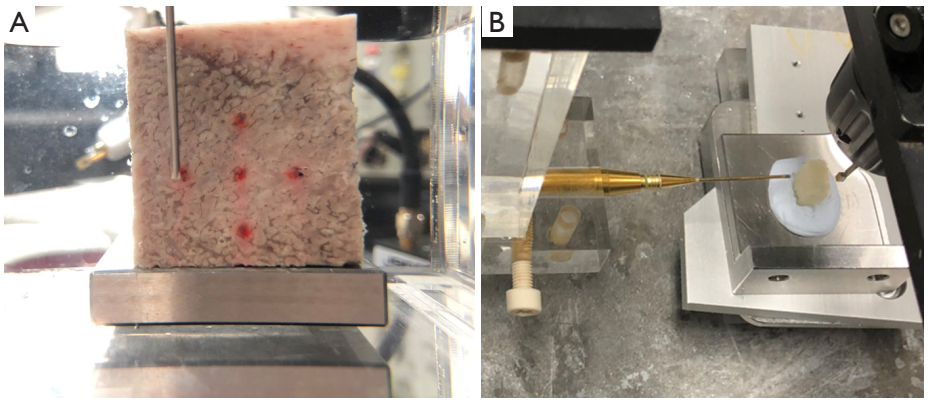

Figure 4 Representative image of (A) the backscatter experiment and (B) the transmission experiment.

MATLAB (MathWorks, Natick, MA, USA) was employed for data processing purposes to obtain the filtered echo signal. The influence of interference signal on echo signal could be greatly reduced by data-filtering processing. The peak value of the processed echo data was extracted and is represented as the mean ± standard deviation (SD). Statistical analysis was performed using GraphPad Prism 10.0 software (GraphPad Software). The Pearson correlation coefficient (r) and two-tailed P value were statistically analyzed, and statistical significance was defined as a P value <0.05.

Results

The ultrasonic wave exhibits similar propagation characteristics to light when it vertically interacts with a different medium, resulting in the generation of a reflected wave propagating in the opposite direction and a transmitted wave propagating in the same direction as the incident wave. The experiment involved the incidence of ultrasonic waves on cancellous bone at a vertical angle, thereby eliminating the influence of the ultrasonic incidence angle on experimental results and solely considered the transmission and backscattering characteristics of ultrasonic signals of the bone structure itself. The width of the sound beam gradually increases as the distance of the transmitted sound field increases for the planar transducer, thereby impacting the resolution and energy distribution of the sound field. Consequently, accurate test results are greatly influenced by factors such as the distance between the bone block sample, transducer, and hydrophone, as well as their relative sizes. In order to minimize the impact of bone block edges on ultrasonic wave scattering and diffraction in ultrasonic transmission experiments, the bone sample size used was greater than 20 mm, and the maximum size of the ultrasonic transducer remained below 5 mm, as shown in *Figure 4A*. Additionally, efforts were made to minimize the distance between the transducer's sample, hydrophone, and bone block without compromising signal transmission integrity, as shown in *Figure 4B*. The signal could be distinguished between the echo signal and the near-field oscillation signal in the time domain, which was convenient for later comparison and analysis with the transosseous signal.

The pulse transmission method, using ultrasonic signals of different frequencies, was employed to investigate the acoustic transmission characteristics of cancellous bone across various thicknesses. First, the reference signals received by the hydrophone at each ultrasound frequency were saved without the insertion of the cancellous bone block. Subsequently, while maintaining a constant relative distance between the transducer and hydrophone, cancellous bone samples of varying thicknesses were inserted between them using the standard substitution method, and the resulting bone transmission signals were recorded. Both the reference signal and bone transmission signal were analyzed in the time domain. The statistical results of ultrasonic characteristics data for various cancellous bone samples with different ultrasound frequencies are presented in *Table 3*. The error of the average sound speed measured by a multilayer and multi-ROI statistical method was less than 10%. The sound attenuation coefficient in the frequency range of 2–3 MHz was below 10 dB/cm. The accuracy of experimental data were primarily influenced by the test conditions, signal postprocessing threshold, and ROIs. Additionally, the noise signal level and transmitted signal amplitude also exerted a degree of influence on the results.

Table 3 Acoustic properties of different cancellous bones

Frequency, MHz	Sample	c_S, m/s			$\alpha(f)$, dB/cm		
		Min–max	Mean	SD	Min–max	Mean	SD
2.2	BSS2	1,312.8–1,573.2	1,456.1	67.4	6.9–11.7	9.2	1.2
	BSS3	1,282.9–1,573.4	1,445.5	78.5	6.1–11.9	9.2	1.7
	HAB4	1,141.2–1,691.6	1,334.6	91.1	3.2–7.9	5.6	1.4
	HAB5	1,245.7–1,557.5	1,431.6	120.2	1.9–10.2	5.7	2.9
2.5	BSS2	1,372.7–1,578.3	1,472.7	75.9	4.2–13.2	8.6	3.1
	BSS3	1,370.0–1,579.3	1,474.1	76.2	4.8–14.4	9.2	3.4
	HAB4	1,284.6–1,525.9	1,413.3	93.4	3.8–6.6	5.3	1.0
	HAB5	1,371.8–1,487.1	1,445.1	32.5	1.7–5.7	3.6	1.8
3	BSS2	1,059.7–1,606.9	1,327.1	28.2	4.4–8.2	5.9	0.6
	BSS3	1,233.2–1,606.9	1,359.2	45.3	4.9–8.1	6.5	0.9
	HAB4	1,206.9–1,552.6	1,328.1	62.6	4.7–6.5	5.6	0.5
	HAB5	1,201.1–1,520.8	1,435.6	58.0	1.0–3.9	1.7	0.8
12	BSS2	1,337.7–1,537.1	1,418.5	30.7	36.5–41.8	52.9	0.6
	BSS3	1,328.2–1,437.1	1,360.5	14.4	48.2–60.4	52.9	0.7
	HAB4	1,294.9–1,427.4	1,366.7	34.2	50.7–53.8	55.8	5.5
	HAB5	1,246.5–1,492.8	1,366.5	30.8	50.7–53.7	37.6	0.9

SD, standard deviation; BSS, bovine spine specimen; HAB, human vertebral allograft bones.

At 12 MHz, the sound attenuation coefficient increased sharply, up to 55.8 dB/cm.

The amplitude of the ultrasonic transmission signal decreased as the thickness of the cancellous bone sample increased, as shown in *Figure 5*. Moreover, there was no significant difference in the amplitude of the ultrasonic signal transmitted by the two bovine bones at different thicknesses, and the amplitude was significantly lower than that of the human allograft bones. The ultrasonic signal amplitude of the 2.5-MHz transducer exceeded that of the 2.2- and 3-MHz probes due to its larger radiation area, which was respectively 2.56 and 5.56 times greater than those of the other probes, resulting in stronger ultrasound signals being emitted. However, in order to achieve miniature size at low frequencies, the design of the 2.2- and 3-MHz ultrasonic probes compromised the probe's vibration efficiency, resulting in a slightly lower transmitted signal amplitude compared to that at 12 MHz. The aforementioned results demonstrate that low-frequency and high-power ultrasound possess certain advantages in terms of the penetration depth of cancellous bone. Specifically, when subjected to low-frequency ultrasound signals ranging from 2 to 3 MHz, the cancellous bone samples exhibited a maximum penetration depth of approximately 5 mm, accompanied by distinct ultrasonic signal observations.

For homogeneous media, the sound velocity and attenuation are constant values. However, cancellous bone is a highly heterogeneous and anisotropic medium. The closer the cancellous bone is to the cortical bone, the denser the cancellous bone is. Therefore, in this experiment, the sound velocity and attenuation of cancellous bone of different thicknesses showed significant variations. In order to further study the ultrasound characteristics of bone tissue, we conducted ultrasound backscatter experiments.

For the backscatter experiments, the BSS1 was detected at 2.2, 3, 12, and 30 MHz. Due to the low echo amplitude of the 30-MHz ultrasound signal, HAB1–3 were subjected to testing at frequencies of 2.2, 3, and 12 MHz, respectively. The statistical analysis results of ultrasonic backscattering experiments on multiple ROIs of different bone samples and at different thicknesses at different ultrasound frequencies are shown in *Table 4*. The relationship between mean ± SD

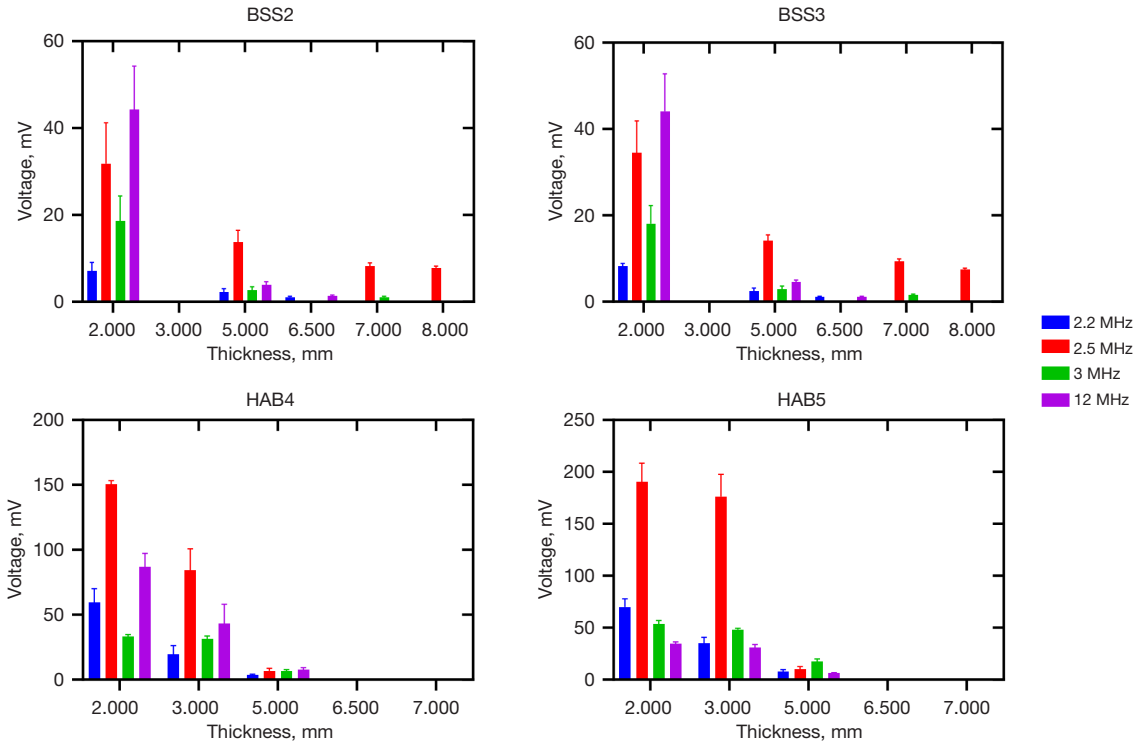

Figure 5 The relationship between the cancellous bone thickness and amplitude of transmitted signal at different frequencies. BSS, bovine spine specimen; HAB, human vertebral allograft bone.

and the thickness of the bone sample is shown in *Figure 6*. The BSS1 exhibited consistent results at frequencies of 12 and 30 MHz, and as the thickness of the cancellous bone layer on the cortical bone decreased, there was a noticeable increase in the amplitude of the echo signal. However, the amplitude of the 2.2-MHz ultrasonic echo signal exceeded 6.5 mm when the thickness was 8 mm, and the amplitude of the 3-MHz ultrasonic echo signal at 6.5 and 3 mm was lower than that of the previous thickness. The potential factors contributing to this include measurement error and the disparity in size between the bovine bone sample and the transducer. Despite marking each measurement with a red box, we faced difficulty in ensuring consistent detection orientation across different thicknesses. The echo signal amplitude of the same bone sample gradually increased as the thickness of the cancellous bone layer on the cortical bone decreased at frequencies of 2.2, 3, and 12 MHz.

The amplitude of echo under the same ultrasound frequency and different bone sample thickness was subjected to statistical analysis, which included calculating the Pearson correlation coefficient (r) and determining the two-tailed P value; the results are shown in *Table 5*. The P values for all comparisons were found to be less than 0.05, indicating significant differences in the amplitude between different groups with varying bone sample thicknesses. The correlation coefficient (r) between ultrasonic echo amplitude and bone sample thickness exhibited a negative relationship, with an average value of –0.84.

The amplitude of the ultrasonic echo signal of different ROIs within the same bone sample exhibited significant variations. For example, in BSS1, the ultrasonic frequency employed was 3 MHz, while the thickness of BSS1 measured 5 mm. The echo signal amplitudes for ROI-1 and ROI-2 are 0.77 and 1.56 V, respectively, exhibiting an amplitude difference of roughly one-fold, as shown in *Figure 7*. The selection of ROIs significantly influenced the experimental result; therefore, it is imperative to mitigate experimental errors by averaging results obtained from multiple ROI measurements. At the same center frequency, the ultrasonic echo characteristics of different bone samples varied with the sample thickness, as shown in *Figure 8*. The echo amplitude of BSS1 was found to be higher than that of the HAB samples under the same ultrasonic frequency and bone sample thickness. However, no significant difference

Table 4 Statistical results of the ultrasonic backscattering experimental data

Bone sample	Thickness (mm)	2.2 MHz	3 MHz	12 MHz	30 MHz
BSS1	2	1.86±0.11	2.21±0.29	1.39±0.24	0.23±0.10
	3	1.18±0.08	1.01±0.22	0.72±0.17	0.16±0.03
	5	0.95±0.36	1.12±0.4	0.32±0.07	0.08±0.01
	6.5	0.56±0.03	0.57±0.16	0.38±0.05	0.08±0.01
	8	0.76±0.12	0.64±0.13	0.23±0.03	0.06±0.01
HAB1	1	2.72±0.28	2.52±0.35	2.24±0.30	–
	4	0.47±0.07	0.58±0.10	0.30±0.05	–
	6	0.29±0.05	0.31±0.05	0.34±0.10	–
	8	0.30±0.03	0.35±0.06	0.14±0.04	–
HAB2	1.5	1.43±0.35	2.01±0.36	1.21±0.17	–
	4	0.90±0.18	0.92±0.33	0.33±0.06	–
	6	0.44±0.10	0.35±0.11	0.20±0.03	–
	8	0.28±0.04	0.24±0.06	0.16±0.04	–
HAB3	2	2.50±0.38	2.34±0.40	1.37±0.65	–
	4	0.35±0.07	0.28±0.08	0.17±0.04	–
	6.5	0.26±0.06	0.34±0.07	0.14±0.04	–

Data are presented as mean ± standard deviation. BSS, bovine spine specimen; HAB, human vertebral allograft bones.

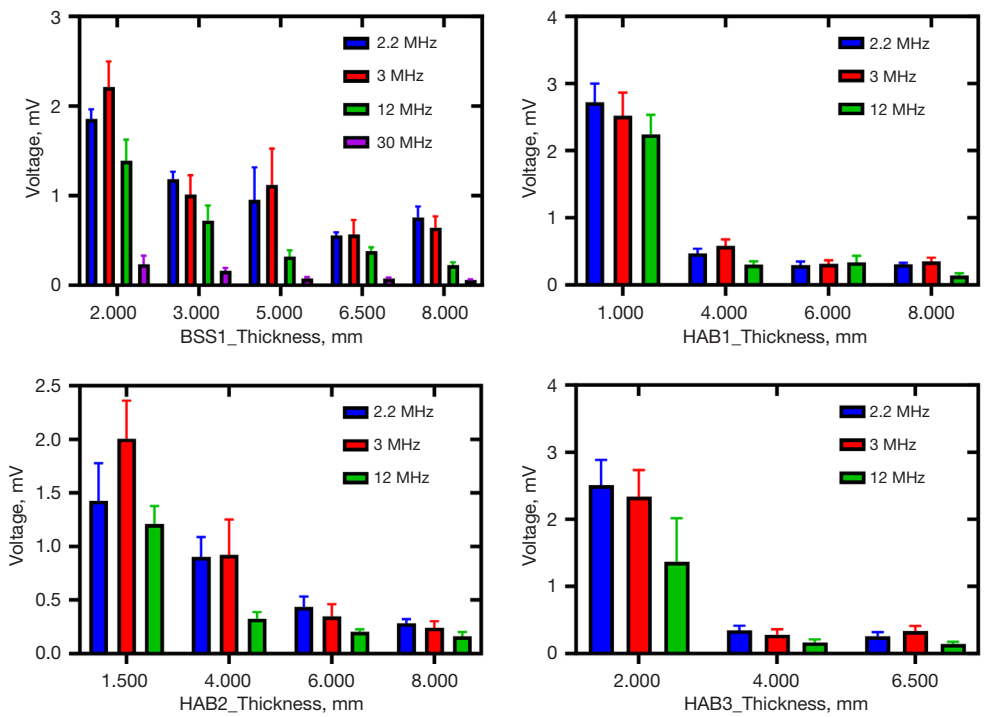

Figure 6 The results of ultrasonic echo signal amplitude variation with the thickness of the cancellous bone layer on the cortical bone. BSS, bovine spine specimen; HAB, human vertebral allograft bone.

Table 5 Correlation and P value of ultrasonic backscatter characteristics

Bone sample	2.2 MHz	3 MHz	12 MHz	30 MHz
BSS1	0.83/0.0001	0.77/0.0007	−0.84/<0.0001	0.8/0.0003
HAB1	−0.86/<0.0001	−0.87/<0.0001	−0.86/<0.0001	–
HAB2	−0.91/<0.0001	−0.91/<0.0001	−0.87/<0.0001	–
HAB3	0.84/0.0001	0.8/0.0003	0.73/0.0022	–

Data are presented as r/P. BSS, bovine spine specimen; HAB, human vertebral allograft bone; r, Pearson correlation coefficient; P, P value.

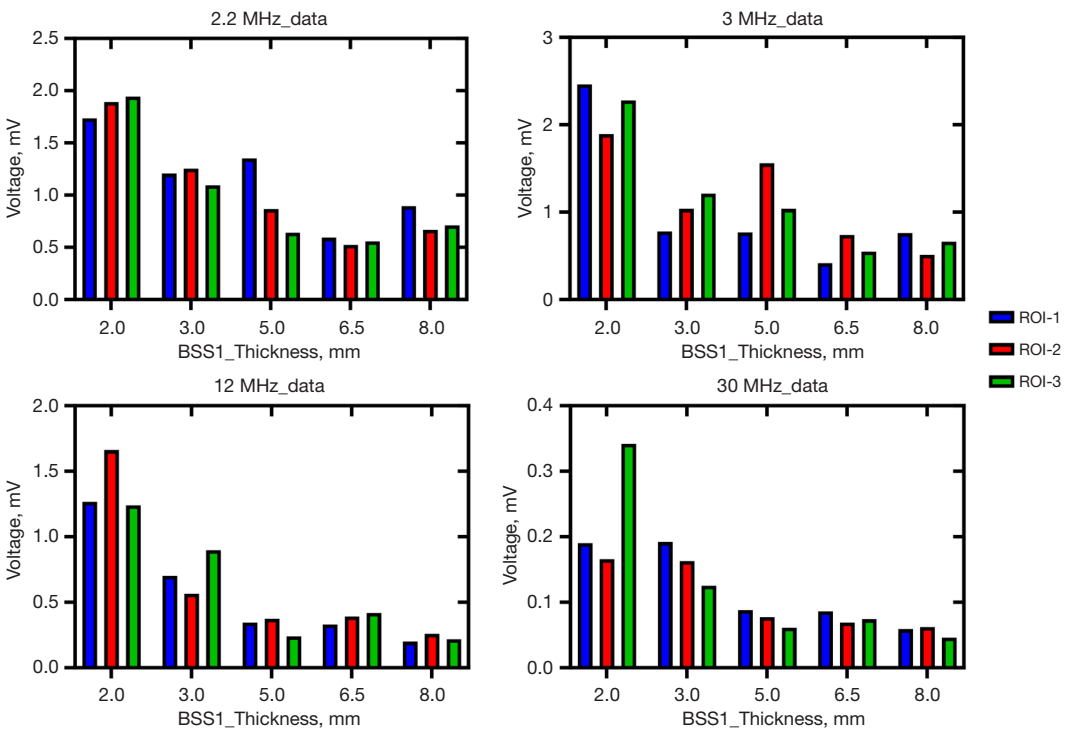

Figure 7 The relationship between the BSS1_thickness and amplitude of ultrasonic echo signal at different ROI. ROI, region of interest; BSS, bovine spine specimen.

in echo amplitude was observed between the HAB samples and BSS1 when only cortical bone with similar thickness was present.

Cancellous bone is a porous or reticular structure formed by the interlacing of anisotropic trabeculae. The material properties, orientation, and degree of anisotropy of the trabeculae significantly impact the ultrasonic transmission and backscattering characteristics. To further investigate the correlation between bone microstructure and ultrasonic backscattering properties, micro-CT scanning of BSS1 was conducted using Skyscan 1174 (Bruker). The schematic diagram of the micro-CT is presented in *Figure 9*, with the specific steps of implementation being as follows: (I) the CT Analyser (version: 1.13.10.1; Bruker, Billerica, MA, USA) identified and delineated three calculation areas (ROI-1, ROI-2, and, ROI-3) as 5×5 mm squares on the surface of cancellous bone. (II) The CT data of the cancellous bone layer with thicknesses of D1 (4.83 mm), D2 (3.32 mm), and D3 (1.81 mm) were acquired at each ROI. (III) The acquired CT data of the ROIs, with consistent thickness, were subjected to statistical analysis to determine the mean ± SD. (IV) The cortical bone layer exhibited a compact structure with minimal regional variations in bone density, and to facilitate calculations, the CT data of a rectangular

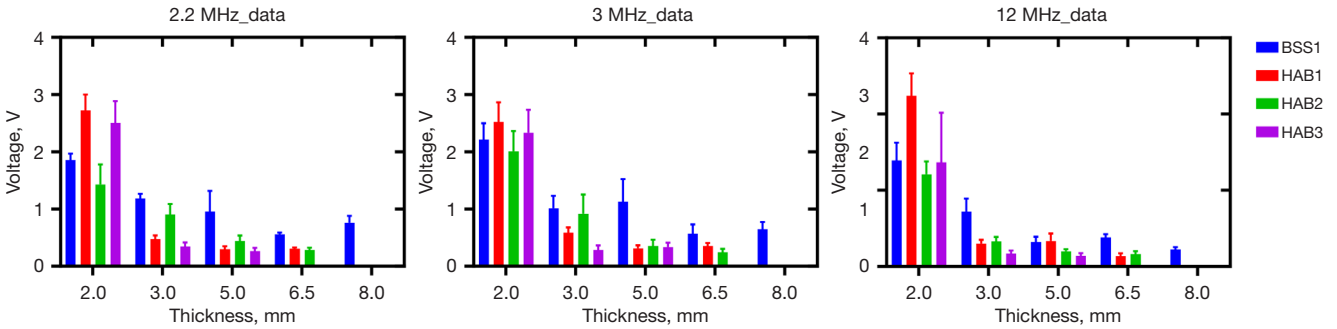

Figure 8 The relationship between the thickness of bone samples and amplitude of ultrasonic echo signal at the same ultrasound frequency. BSS, bovine spine specimen; HAB, human vertebral allograft bone.

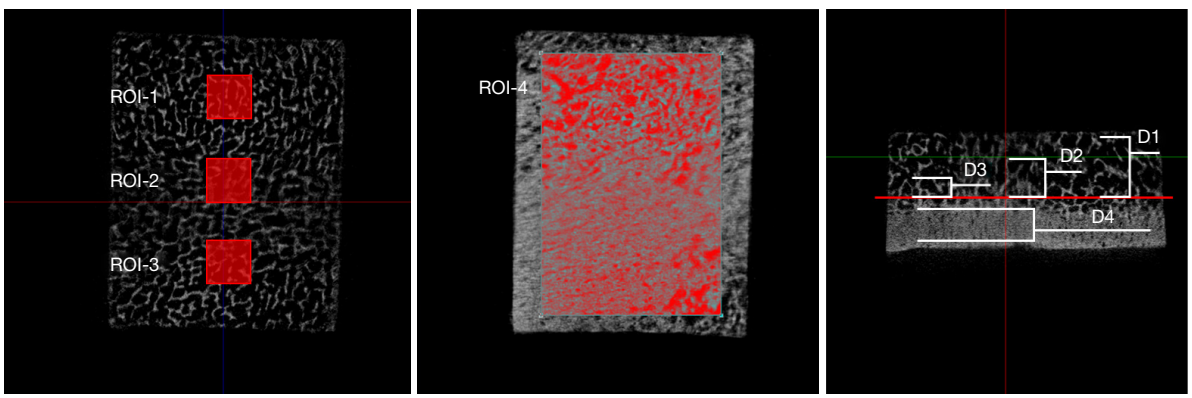

Figure 9 The schematic diagram of the micro-CT for BSS1. ROI, region of interest; D1, cancellous bone thickness (4.83 mm); D2, cancellous bone thickness (3.32 mm); D3, cancellous bone thickness (1.81 mm); D4, cortical bone thickness (4.83 mm); CT, computed tomography; BSS, bovine spine specimen.

Table 6 The micro-CT statistical results of BSS1

Depth (mm)	BV/TV (%)	Tb.Pf (1/mm)	SMI	Tb.Th (mm)	Tb.N (1/mm)	Tb.Sp (mm)
D1 (4.83)	16.57±1.52	4.92±1.17	2.01±0.32	0.21±0.005	0.80±0.06	0.68±0.005
D2 (3.32)	18.07±2.11	4.52±1.37	1.93±0.33	0.21±0.01	0.87±0.07	0.64±0.01
D3 (1.81)	19.40±2.62	4.64±1.47	1.92±0.31	0.20±0.013	0.95±0.07	0.59±0.03
D4 (2.72)	93.78	−33.75	−30.72	0.57	1.64	0.11
r	−0.82	0.81	0.80	−0.80	−0.88	0.87

Continuous variables are presented as the mean ± standard deviation. CT, computed tomography; BSS, bovine spine specimen; BV/TV, bone volume/tissue volume; Tb.Pf, trabecular pattern factor; SMI, structure model index; Tb.Th, trabecular thickness; Tb.N, trabecular number; Tb.Sp, trabecular separation; D1, cancellous bone thickness (4.83 mm); D2, cancellous bone thickness (3.32 mm); D3, cancellous bone thickness (1.81 mm); D4, cortical bone thickness (2.72 mm); r, Pearson correlation coefficient.

area 17.5 mm × 25 mm in size and with a thickness of D4 (2.72 mm) were averaged. The CT statistical results of BSS1 and the Pearson correlation coefficient (r) are shown in the *Table 6*, which include bone volume/tissue volume (BV/TV; %), trabecular pattern factor (Tb.Pf; 1/mm), structure model index (SMI), trabecular thickness (Tb.Th; mm), trabecular number (Tb.N; 1/mm), and trabecular separation (Tb.Sp; mm).

The regions labeled for micro-CT data analysis coincided with those designated for ultrasound irradiation in backscattering experiments. The CT data in *Table 6* reveal that as the proximity of cortical bone increased, there was a corresponding increase in BV/TV and Tb.N. Specifically, BV/TV, Tb.Th, and Tb.N were 4.8, 2.8, and 1.7 times greater in cortical bone compared to cancellous bone, respectively. The Tb.Sp decreased the closer it came to the cortical bone, with the Tb.Sp of cortical bone being only 18% of the cancellous bone. The correlation coefficient (r) between the bone structural parameters and distribution of cancellous bone samples exhibited a high correlation, meaning that the closer to cortical bone it was, the denser the bone tissue. The r values of Tb.Sp and Tb.N were relatively higher, and thus can be used to characterize changes in bone tissue structure. Furthermore, the overall tendency of the ultrasonic backscattering test results (*Figure 7*) aligns with that of the micro-CT scan results (BV/TV, Tb.Pf , Tb.Th, and Tb.N). The result shows that both the ultrasonic characteristics and micro-CT data of bone sample were closely associated with the distribution of cancellous bone samples. The micro-CT scan results effectively validated the ultrasonic test findings, and to some extent, changes in bone microstructure can be inferred from the ultrasonic test outcomes. The findings hold significant clinical implications, as there is potential for ultrasound detection of bone tissue to supplant CT scans in the future.

Discussion

The use of low-frequency, high-power ultrasound offers significant advantages in terms of the penetration depth within cancellous bone (25,26). Specifically, when employing a low-frequency ultrasonic signal ranging from 2 to 3 MHz, it is possible to penetrate cancellous bone samples with a maximum thickness of approximately 5 mm while simultaneously observing distinct transmission ultrasonic signals. The ultrasound signals at frequencies of 12 and 30 MHz undergo significant attenuation when passing through cancellous bone, primarily within the cancellous bone itself. Consequently, it is difficult for high-frequency ultrasonic signals to effectively penetrate cancellous bone. In our study, the amplitude of the echo signal at the cancellous bone interface progressively increased as the thickness of the cancellous bone layer on the cortical bone decreased. When there was minimal presence of a cancellous bone layer on the cortical bone, the amplitude of the echo signal exhibited an exponential increase. The amplitude of ultrasound echo signals increased as it approached the cortical bone, with similar changes observed in the micro-CT scan results. Therefore, to some extent, ultrasound detection results and CT scan results can validate each other. Theoretically, it is possible to employ multiple ultrasonic probes (≥3) and multiple ROIs (≥5) for the detection of the pedicle screw channel, and the ultrasonic echo signal amplitude can be monitored for any consecutive increase of more than 3 times or sudden substantial increases, serving as an early warning indicator to alert surgeons of potential pedicle perforation. The findings of our study align with the results presented in the previous studies (27,28).

In order to reduce the interference of various factors in the actual pedicle screw path, our experiment mainly focused on the quantitative analysis of ultrasonic propagation characteristics of bone tissue. The circumferential wall of the pedicle screw path in actual clinical practice, however, exhibits irregular shape and is filled with blood and bone particles. Additionally, the human body temperature is around 37 ℃, whereas the experiments were conducted in a 25 ℃ environment. The speed of sound differs under different temperatures, which is another limitation of this study. As a result, the ultrasound navigation environment is significantly more complex than that observed in this experiment. Therefore, further investigative efforts are imperative to establish the safety of relying exclusively on ultrasound guidance for pedicle screw fixation procedures. In the subsequent research phase, we will aim to enhance the performance of low-frequency micro ultrasonic transducers and focus on conducting ultrasonic imaging experiments in complex pedicle environments, such as those containing blood, bone fragments, and other debris. Moreover, we will use a wider range of experimental approaches and techniques to acquire more robust and reliable data that closely reflect the clinical reality, thereby further validating the findings derived from this study. The primary objective is to supplant CT navigation with ultrasound guidance, thereby diminishing the risks associated with CT radiation exposure for both surgeons and patients. Moving forward, our plan involves seamlessly integrating miniature ultrasound probes at the tip of the dilator and ensuring there is no disruption to surgical protocols or added complexity for surgeons. This seamless integration will provide real-time feedback on the trajectory of the screw pathway during pedicle drilling, equipping surgeons with crucial warning alerts and precise guidance for the drilling direction.

Acknowledgments

Funding: This work was supported by Social Development in Jiangsu Clinical Frontier Technology (No. BE2021659), the National Key Research and Development Program of China (No. 2022YFF0706500), the Suzhou Science and Technology Plan Project (Nos. SJC2022010, SZS2022008), the Quancheng 5150 Project, and the University Synergy Innovation Program of Anhui Province (No. GXXT-2022-048).

Footnote

Conflicts of Interest: All authors have completed the ICMJE uniform disclosure form (available at https://qims.amegroups.com/article/view/10.21037/qims-24-377/coif). W.L. is an employee of Suzhou GuoKe Ultra Medical Technology Co., Ltd. The other authors have no conflicts of interest to declare.

Ethical Statement: The authors are accountable for all aspects of the work in ensuring that questions related to the accuracy or integrity of any part of the work are appropriately investigated and resolved. Since the bone samples used in this study were commercial bone blocks and did not involve any animal or human experimentation. Therefore, it was not necessary to obtain approval from the Animal Ethics Review Board and the Human Research Ethics Committee.

References

1. Weinstein JN, Rydevik BL, Rauschning W. Anatomic and technical considerations of pedicle screw fixation. Clin Orthop Relat Res 1992;(284):34-46.
2. Li HM, Zhang RJ, Shen CL. Accuracy of Pedicle Screw Placement and Clinical Outcomes of Robot-assisted Technique Versus Conventional Freehand Technique in Spine Surgery From Nine Randomized Controlled Trials: A Meta-analysis. Spine (Phila Pa 1976) 2020;45:E111-9.
3. Chen L, Xu L, Qiu Y, Qiao J, Wang F, Liu Z, Shi B, Qian BP, Zhu Z. The risks of aorta impingement from pedicle screw may increase due to aorta movement during posterior instrumentation in Lenke 5C curve: a computed tomography study. Eur Spine J 2015;24:1481-9.
4. Kapoen C, Liu Y, Bloemers FW, Deunk J. Pedicle screw fixation of thoracolumbar fractures: conventional short segment versus short segment with intermediate screws at the fracture level-a systematic review and meta-analysis. Eur Spine J 2020;29:2491-504.
5. Ding H, Hai Y, Liu Y, Guan L, Pan A, Zhang X, Han B, Li Y, Yin P. Cortical Trajectory Fixation Versus Traditional Pedicle-Screw Fixation in the Treatment of Lumbar Degenerative Patients with Osteoporosis: A Prospective Randomized Controlled Trial. Clin Interv Aging 2022;17:175-84.
6. Chan A, Parent E, Lou E. Reconstruction and positional accuracy of 3D ultrasound on vertebral phantoms for adolescent idiopathic scoliosis spinal surgery. Int J Comput Assist Radiol Surg 2019;14:427-39.
7. Chan A, Parent E, Narvacan K, San C, Lou E. Intraoperative image guidance compared with free-hand methods in adolescent idiopathic scoliosis posterior spinal surgery: a systematic review on screw-related complications and breach rates. Spine J 2017;17:1215-29.
8. Mueller CA, Roesseler L, Podlogar M, Kovacs A, Kristof RA. Accuracy and complications of transpedicular C2 screw placement without the use of spinal navigation. Eur Spine J 2010;19:809-14.
9. Modi H, Suh SW, Song HR, Yang JH. Accuracy of thoracic pedicle screw placement in scoliosis using the ideal pedicle entry point during the freehand technique. Int Orthop 2009;33:469-75.
10. Feng W, Wang W, Chen S, Wu K, Wang H. O-arm navigation versus C-arm guidance for pedicle screw placement in spine surgery: a systematic review and meta-analysis. Int Orthop 2020;44:919-26.
11. Gueziri HE, Santaguida C, Collins DL. The state-of-the-art in ultrasound-guided spine interventions. Med Image Anal 2020;65:101769.
12. Al-Habib AF, Al-Akkad S. Segmental Surface Referencing during Intraoperative Three-dimensional Image-Guided Spine Navigation: An Early Validation with Comparison to Automated Referencing. Global Spine J 2016;6:765-70.
13. Overley SC, Cho SK, Mehta AI, Arnold PM. Navigation and Robotics in Spinal Surgery: Where Are We Now?

Neurosurgery 2017;80:S86-99.
14. Wu T, Chen YF, Huang Y, Meng FH, Lu JH, Liu D. Ultrasound-guided Jamshidi needle puncture to reduce radiation exposure during percutaneous pedicle screw placement: study protocol for a randomised controlled trial. BMJ Open 2023;13:e064838.
15. MacLean LJ, Street J, Hodgson AJ. Design of an ultrasound-emitting drill guide for freehand pedicle screw navigation. Int J Med Robot 2023;19:e2555.
16. Gueziri HE, Georgiopoulos M, Santaguida C, Collins DL. Ultrasound-based navigated pedicle screw insertion without intraoperative radiation: feasibility study on porcine cadavers. Spine J 2022;22:1408-17.
17. Barkmann R, Glüer CC. Clinical Applications. In: Laugier P, Haïat G, editors. Bone Quantitative Ultrasound. Dordrecht: Springer Netherlands, 2011:73-81.
18. Zhang H, Wu S, Ta D, Xu K, Wang W. Coded excitation of ultrasonic guided waves in long bone fracture assessment. Ultrasonics 2014;54:1203-9.
19. Yang C, Li P, Cui Y, Shao W, Wang N, Shen J. A Dual-frequency Probe with Coded Excitation for Ultrasound Guided Screw Insertion in Spinal Fusion Surgery. 2020 IEEE International Ultrasonics Symposium (IUS), Las Vegas, NV, USA, 2020:1-4.
20. Petrone B, Albano J, Stockton R, Atlas AM, Aronica C, Grewal K. Demographic Analysis of Pedicle Diameter, and Estimated Pedicle Screw Length of the Lumbar Spine in a Diverse Population. Int J Spine Surg 2021;15:259-65.
21. Mujagić M, Ginsberg HJ, Cobbold RS. Development of a method for ultrasound-guided placement of pedicle screws. IEEE Trans Ultrason Ferroelectr Freq Control 2008;55:1267-76.
22. Droin P, Berger G, Laugier P. Velocity dispersion of acoustic waves in cancellous bone. IEEE Trans Ultrason Ferroelectr Freq Control 1998;45:581-92.
23. Wu K, Xue Q, Adler L. Reflection and transmission of elastic waves from a fluid-saturated porous solid boundary. J Acoust Soc Am 1990;87:2349-58.
24. Chaffaï S, Padilla F, Berger G, Laugier P. In vitro measurement of the frequency-dependent attenuation in cancellous bone between 0.2 and 2 MHz. J Acoust Soc Am 2000;108:1281-9.
25. Manbachi A, Lee M, Foster FS, Ginsberg HJ, Cobbold RSC. Design and fabrication of a low-frequency (1-3 MHz) ultrasound transducer for accurate placement of screw implants in the spine. Medical Imaging 2014: Ultrasonic Imaging and Tomography: SPIE, 2014:117-26.
26. Kilappa V, Moilanen P, Xu L, Nicholson PH, Timonen J, Cheng S. Low-frequency axial ultrasound velocity correlates with bone mineral density and cortical thickness in the radius and tibia in pre- and postmenopausal women. Osteoporos Int 2011;22:1103-13.
27. Raphael DT, Chang JH, Zhang YP, Kudija D, Chen TC, Shung KK. A-Mode ultrasound guidance for pedicle screw advancement in ovine vertebral bodies. Spine J 2010;10:422-32.
28. Il Lee K. Relationships of the ultrasonic backscatter measurements with the bone mineral density and the microarchitectural parameters in bovine trabecular bone in vitro. J Acoust Soc Am 2020;148:EL51.

Cite this article as: Li P, Li S, Li Z, Lu W, Shao W, Li Z, Xu Y, Zhang H, Ju B, Shen J, Cui Y. Ultrasound propagation characteristics within the bone tissue of miniature ultrasound probes: implications for the spinal navigation of pedicle screw placement. Quant Imaging Med Surg 2024;14(7):4878-4892. doi: 10.21037/qims-24-377

